Multiparameter estimation of continuous-time quantum walk Hamiltonians through machine learning

Cite as: AVS Quantum Sci. **5**, 014405 (2023); https://doi.org/10.1116/5.0137398
Submitted: 02 December 2022 • Accepted: 07 February 2023 • Published Online: 24 February 2023

Ilaria Gianani and Claudia Benedetti

AVS Quantum Science ARTICLE scitation.org/journal/aqs

Multiparameter estimation of continuous-time quantum walk Hamiltonians through machine learning

Cite as: AVS Quantum Sci. **5**, 014405 (2023); doi: 10.1116/5.0137398
Submitted: 2 December 2022 · Accepted: 7 February 2023 ·
Published Online: 24 February 2023

Ilaria Gianani[1,a] and Claudia Benedetti[2]

AFFILIATIONS

[1]Dipartimento di Scienze, Università degli Studi Roma Tre, Via della Vasca Navale 84, 00146 Rome, Italy
[2]Dipartimento di Fisica "Aldo Pontremoli," Università degli Studi di Milano, 20133 Milan, Italy

[a)]Electronic mail: ilaria.gianani@uniroma3.it

ABSTRACT

The characterization of the Hamiltonian parameters defining a quantum walk is of paramount importance when performing a variety of tasks, from quantum communication to computation. When dealing with physical implementations of quantum walks, the parameters themselves may not be directly accessible, and, thus, it is necessary to find alternative estimation strategies exploiting other observables. Here, we perform the multiparameter estimation of the Hamiltonian parameters characterizing a continuous-time quantum walk over a line graph with n-neighbor interactions using a deep neural network model fed with experimental probabilities at a given evolution time. We compare our results with the bounds derived from estimation theory and find that the neural network acts as a nearly optimal estimator both when the estimation of two or three parameters is performed.

I. INTRODUCTION

The characterization and control of quantum processes is a fundamental requirement for the realization of quantum protocols and crucial for the development of quantum technologies.[1–3] Controlling and validating the dynamics of quantum systems, i.e., their Hamiltonian, is a computationally demanding task to perform with classical resources, but can be mitigated by the use of Machine Learning (ML).[4–6] ML techniques have been proven to be of substantial aid when adapted to quantum states characterization,[7–14] optimization of control strategies,[15–18] quantum state transport[19,20] as well as for parameter estimation and classification tasks.[21–28] Concerning the characterization of quantum processes, Hamiltonian learning strategies have been extensively investigated in order to provide a reliable solution to this challenge.[29–34] Moreover, it is pivotal that the required information is often not directly accessible and must be inferred starting from experimental quantities.[35,36]

For parametrized Hamiltonians, this translates in establishing the values of significant Hamiltonian parameters starting from measured quantities. This task is akin to what pertains quantum metrology[37–40] and can be cast in terms of the multiparameter estimation theory.[41] In the estimation framework, Neural Networks (NNs) have demonstrated to achieve superior performance in terms of reliability with finite-size dataset and robustness to noise compared to standard estimators,[22] and as such, they appear as a primary candidate for successfully estimating parametrized Hamiltonians.

In the class of parametrized Hamiltonians, an exceptionally diffused and useful example is that of quantum walks (QWs). QWs are a universal and versatile tool that can be harnessed to perform a plethora of tasks ranging from energy transport[42–44] to quantum algorithms,[45–51] quantum computation,[52–54] and quantum communication.[55] In particular, continuous-time quantum walks (CTQWs) are the quantum analog of classical random walks[56–59] that describe the continuous evolution of a quantum particle over a set of discrete positions. These positions can be pairwise linked in different ways, generating graphs with different topologies. Indeed, the edges of a graph identify all the possible paths that the quantum particle can walk through. The edges weights, together with the on-site energies, are the relevant parameters characterizing the CTQW Hamiltonian.

CTQWs are especially useful to model physical phenomena such as quantum transport of energy in quantum biological systems, quantum routing, and quantum state transfer.[60–66] They have been both realized and simulated experimentally on different platforms, such as photons,[67–69] trapped atoms and ions,[70,71] waveguide arrays,[72–75] microwaves,[76] and nuclear magnetic resonance.[77]

In all these tasks, fine tuning of the Hamiltonian parameters is required in order to achieve reliable and satisfactory results.[78–81] The control of experimental CTQWs usually relies on a set of directly accessible experimental parameters, which indirectly dictate the values of the Hamiltonian ones. However, since the mapping between these two sets of parameters can be particularly involved, in order to reliably characterizing the Hamiltonian, a detailed calibration linking one set to the other may not be sufficient. Hamiltonian learning strategies must, hence, be developed, estimating the relevant Hamiltonian parameters starting from experimental observables.

Here, we discuss how to successfully address the characterization of the CTQW Hamiltonian as an estimation problem in a network with a fixed topology. In particular, we explore how to infer the Hamiltonian parameters of a CTQW unfolding on a line graph with n-neighbor interactions, having access only to the probability distribution on the graph's sites at a known time t and to the initial state of the system. By casting the problem in informational terms, we determine the most suitable measurement configuration and then perform the estimation with a Deep Neural Network model. Our results show that our model acts as a nearly optimal estimator, saturating the bounds established by the estimation theory.

II. RESULTS

A. Multiparameter estimation of CTQW

CTQWs describe the evolution of a quantum particle that coherently moves among a set of N_s discrete positions $\{|x\rangle\}_{x=1}^{N_s}$, which constitute a basis for the CTQW Hilbert space. The Hamiltonian generating the quantum dynamics is expressed in terms of on-site energies ϵ_x and couplings J_{xy} between sites x and y. Here, we focus on a CTQW on a line with zero on-site energies $\epsilon_x = 0\,\forall x$ and n-neighbor uniform couplings, such that the Hamiltonian can be written as

$$H = -\sum_{i=1}^{n}\sum_{x}^{N_s-i} J_i(|x+i\rangle\langle x| + |x\rangle\langle x+i|). \tag{1}$$

In this work, the couplings J_i are taken to be positive real numbers. This model could be generalized by considering complex couplings, which lead to chiral QWs.[82–86] Given the Hamiltonian (1) and an initial state of the walker $|\psi_0\rangle$, the evolution of the CTQW at time t is generated by the operator e^{-iHt}, such that the probability of occupying site x is expressed as

$$p_x(t, J_1, \ldots, J_n) = |\langle x|e^{-iHt}|\psi_0\rangle|^2. \tag{2}$$

The squared norm operation in Eq. (2) establishes a non-linear mapping between its Hilbert space and the probability distributions in position space; this non-linearity, together with a high sensitivity to the initial condition, is linked to a chaotic behavior of QWs that can be exploited to build secure cryptographic protocols.[87–89]

The main objective of this work is described in Fig. 1: our graph is a chain with N_s sites, and the CTQW Hamiltonian is defined by n parameters J_i, each varying in a known interval which we set as [0,1]. We assume to have control on the initial state $|\psi_0\rangle$ and to have access to the probability $p_x(t, J_1, \ldots, J_n)$ measured at a given time t. We aim at estimating the Hamiltonian parameters $J_1, \ldots, J_n$. As stated before, this problem is highly non-linear, making a direct inversion a complex task. When the Hamiltonian depends only on one parameter, i.e., only uniform first neighbor couplings are considered, it is possible to address the problem analytically.[90,91] Since we are dealing with an arbitrary large but finite number of parameters, we can cast this problem in terms of multiparameter estimation, and, given that our measurement strategy is fixed, i.e., we are performing a position measurement over all the sites of the chain, we can directly refer to the classical Fisher Information (FI). In this scenario, the FI is a matrix of dimension $n \times n$ whose elements are defined as

$$F_{ij} = \sum_x \frac{\partial_{J_i} p_x(t, J_1, \ldots, J_n)\partial_{J_j} p_x(t, J_1, \ldots, J_n)}{p_x(t, J_1, \ldots, J_n)}. \tag{3}$$

By inverting the FI matrix, we can then cast the Carmér–Rao bound (CRB), lower bounding the variance of the estimated parameters $\Delta^2 J_i$ as

$$M \cdot \Delta^2 J_i \geq (F^{-1})_{ii}, \tag{4}$$

where M is the total resources employed for the measurement. This will serve as a reference to quantify the performance of our estimation. The CRB can always be saturated with an unbiased estimator. Estimation protocols conventionally make use of the maximum likelihood or Bayesian strategies in order to derive an unbiased estimator.[39,92] Machine Learning techniques have recently shown to provide a suitable alternative, allowing to perform optimal estimation without recurring to a detailed model of the problem at hand. Specifically, Neural Networks (NNs) have been used both in single and multiparameter estimations demonstrating to successfully perform optimal estimation when trained with a sufficiently sampled dataset.[22,25] Furthermore, NNs have proven higher robustness to noise compared to the other techniques. This black-box approach is particularly helpful in our scenario as, for most instances, $p_x(t, J_1, \ldots, J_n)$ cannot be evaluated analytically. This complicates the use of traditional estimators in that the probabilities need to be sampled numerically. This issue is usually circumvented by employing Markov chain Monte Carlo methods[93] to evaluate an estimator by sampling the numerical

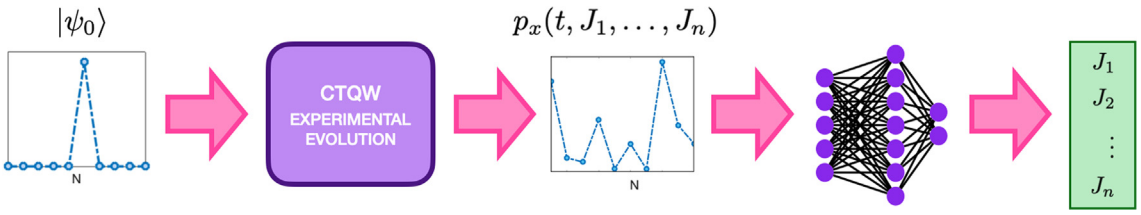

FIG. 1. Conceptual scheme. Starting from a given initial state, a system undergoes a CTQW, and the position probabilities at a time t are recorded. These are then used as input for a deep neural network, which outputs the values of the Hamiltonian parameters defining the CTQW.

probability distributions; however, contrary to the NN approach, these methods rely individually on punctual estimations of the probability distribution and may introduce biases in the estimation, which need to be accounted for.[94]

The CRB in Eq. (4) will depend on all the Hamiltonian parameters J_i as well on other parameters defining the evolution, i.e., the evolution time t and the chain length N_s. Before moving onto the estimation of the Hamiltonian parameters J_i, we, thus, need to set a value for these other parameters by finding a viable regime in which to perform the estimation, dictated by the maximum amount of information extractable. For the sake of simplicity, we consider $n = 2$, so that only the first and second neighbor couplings can be active. This helps in the visualization of the results, but a similar analysis can be carried out with an arbitrary number of parameters. We consider five possible lengths for the chain, $N_s = 5, 10, 20, 30,$ and 100 and five possible evolution times $t = 1, 2, 5, 10,$ and 20 and evaluate the FI elements of Eq. (3) for each combination of N_s and t. The derivatives in Eq. (3) are computed numerically. We consider as the initial state a fourth-order supergaussian with $\sigma = 12$ centered at the center of the chain. This is fixed independently from the chain length. The results are shown in Fig. 2 in panels (a)–(c). Each plot in these panels is a 2D map of F_{ij} as a function of J_1 and J_2. We can draw the following conclusions: at short times and for a short chain, the Fisher information is non zero for both couplings and shows some structure depending on the parameters' values. At short times and for longer chains, the information decreases. This is because at longer lengths, the initial state is not spread across the whole chain, and we are performing a measurement over many sites which have not yet undergone any evolution and, thus, carry little information. This could be mitigated by employing different measurement strategies such as localized measurements

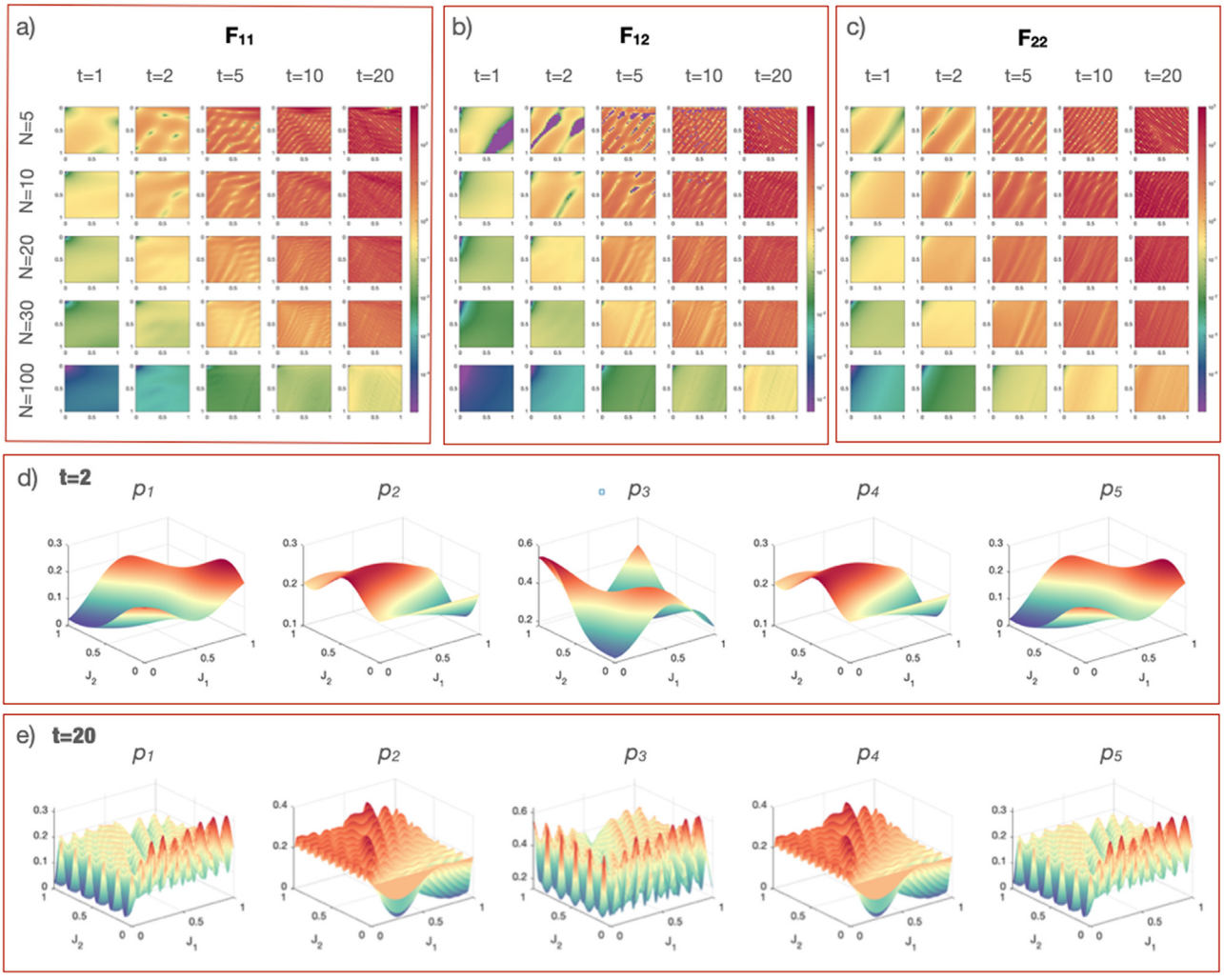

FIG. 2. Information and probability space. Fisher Information Matrix elements, F_{11} (a), F_{22}(b), and F_{33}(c). Each 2D map is the FI element evaluated as a function of the couplings J_1 and J_2 varying in the interval [0,1]. Each element is evaluated for different evolution times (columns) and chain lengths (rows), with $t = 1, 2, 3, 10,$ and 20 and $N_s = 5, 10, 20, 30,$ and 100. Panel (d) shows the five position probabilities p_x for a 5-site chain as a function of the couplings J_1 and J_2 evaluated at time $t = 2$, while panel (e) shows the same probabilities evaluated at time $t = 20$.

addressing only the sites that have undergone the evolution.[90] We note that for longer chain lengths, the information on the second neighbor is consistently higher than that on the first neighbor. This is not surprising, because at any given time, the second neighbor information will have spanned a higher portion of the chain, and, thus, the information would travel faster compared to that of the first neighbor, hence mitigating the decrease in information previously discussed. Finally, we note that increasing the evolution time corresponds to increasing the amount of information, at the cost of the information becoming heavily structured. This reflects the shape of the probability space, shown in Fig. 2 panel (d) and (e), at $t = 2$ and $t = 20$ for $N_s = 5$.

B. Two-parameter estimation

We now proceed with the estimation, while keeping $n = 2$. Based on the results of Fig. 2, we now seek for a combination of chain length and evolution time, where the information on the sought parameters is sufficiently high but not overly structured. Indeed, while it is desirable to have a high information content, a heavily structured profile would be detrimental to the estimation, requiring a tighter sampling of the NN's training dataset. We, hence, fix our chain length to $N_s = 10$ sites and set the evolution time at $t = 1.5$.

In order to perform the estimation, we implement a deep neural network model as follows: the input features are the probabilities of detection at each site x of the chain $p_x(t, J_1, J_2)$; hence, the input layer is comprised of $N_s = 10$ neurons. We then normalize the input features using a Batch Normalization layer, which is followed by six hidden layers of 600 neurons each. The network outputs the value of the two couplings; hence, the output layer will consist of two neurons.

We consider three different initial states $|\psi_0\rangle$: a Gaussian with $\sigma = 0.2$ centered on site $x = 5$ corresponding to a localized excitation,

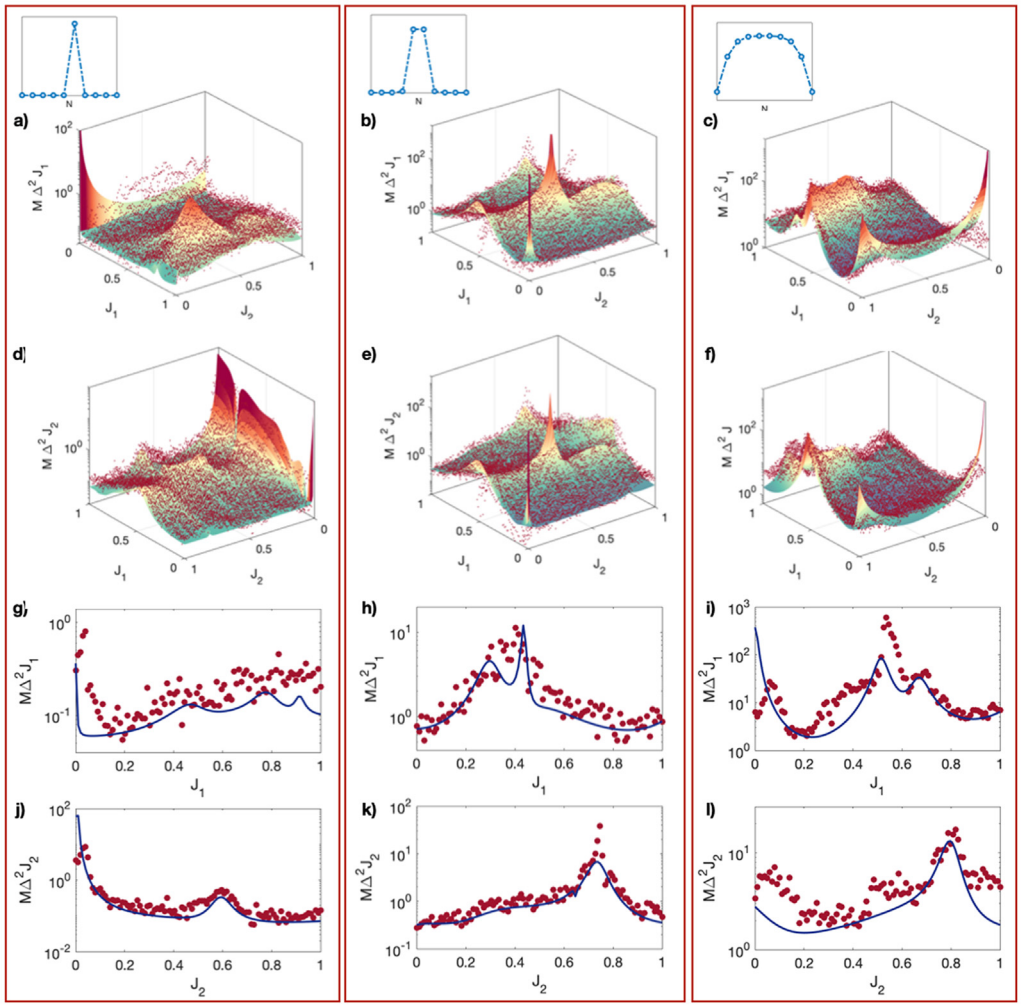

FIG. 3. Two-parameter estimation. Results of the estimation of the first and second neighbor couplings performed using the NN model with three different input states, shown in the inset (columns). Panels (a)–(c) show the log-plots of CRB for J_1 (surface) and the variance of the NN prediction evaluated over the Monte Carlo samples multiplied by the total number of resources M (red circles—see text). Panels (d)–(f) show the log-plots of CRB (surface) and evaluated variance (red circles) for J_2. Panels (g)–(i) show a slice of the 3D plot of $M\Delta^2 J_1$ for $J_2 = 1$, while panels (j)–(l) show a slice of the 3D plot of $M\Delta^2 J_2$ for $J_1 = 1$. In these, the blue line is the CRB, and the red dots are the estimated variances.

a Gaussian with $\sigma = 0.5$ centered at the center of the chain corresponding to an excitation mostly divided between two sites of the graph, and a fourth-order supergaussian with $\sigma = 12$ centered at the center of the chain corresponding to an excitation spread across the whole graph. These are shown in the insets of Fig. 3. Once we have selected the input state, we perform the following procedure for training and testing:

1. we generate $N_{samp} = 2^{14}$ random values for the couple $\{J_1, J_2\}$ uniformly distributed in the extended interval $[-0.2, 1.2]$ in order to limit the bias due to boundary conditions;[22]
2. we use the generated couplings to perform the evolution at time t = 1.5 according to Eq. (2) and record the probability $p_x(t, J_1, J_2)$ for each site x in the chain;
3. we generate simulated counts multiplying the probability $p_x(t, J_1, J_2)$ by the total number of resources which we set at $M = 2 \times 10^5$, so that $\pi_x(t, J_1, J_2) = M \cdot p_x(t, J_1, J_2)$. This puts us in a regime where the CRB should be saturated;
4. in order to account for fluctuations, we bootstrap the training data by running $N_{MC} = 500$ Monte Carlo routines extracting new values $\pi'_x(t, J_1, J_2)$ from a Poisson distribution of mean $\pi_x(t, J_1, J_2)$;
5. we split the generated dataset into the training (0.8) and validation set (0.2);
6. we run the training for 200 epochs with a batch size of 1000 using the Adam optimizer with the learning rate set to 10^{-3} and adopting as metric the MSE.

In order to test the network, we generate a new set of $N_{test} = 10^4$ values of the couples $\{J_1, J_2\}$, now in $[0, 1]$, and evaluate the evolved probabilities, which we multiply by M to simulate the measured counts. We then perform 300 Monte Carlo runs to account for Poissonian noise and use the NN model to predict the values of the couplings for each generated probability. We can then calculate the error on the estimated couplings as the variance $\Delta^2 J_i$ over the Monte Carlo samples and compare it with the CRB, which we obtain from Eq. (4) by inverting the FI matrix of Eq. (3). As for the analysis of Sec. II A, the derivatives of Eq. (3) are evaluated numerically.

The results of the estimation are shown in Fig. 3. The plots show the agreement between the CRB (surfaces) with the variance on estimated values $\Delta^2 J_i$ multiplied by the number of resources M (red dots), indicating that the NN model is able to perform a nearly optimal estimation. The graphs in panels (g)–(l) are slices of the 3D plots for the errors on the first (second) parameter, when the second (first) parameter is taken to be equal to its maximum value, $J_{2(1)} = 1$. The NN model performs comparably for all input states considered.

C. Three-parameter estimation

We now extend the estimation to the case where the CTQW Hamiltonian is defined by three parameters, by considering also the third-neighbor coupling J_3. We keep the chain length fixed at $N_s = 10$ and the evolution time at $t = 1.5$. Since there was no significant discrepancy between the estimations starting with different $|\psi_0\rangle$, we only consider the localized state, i.e., the Gaussian with $\sigma = 0.2$. The NN model we use is the same as for the two-parameter estimation, the only difference being the number of neurons in the output layer, which now amounts to three. The training procedure too remains the same, but since the parameters space has increased, so must the size of the training dataset. We, thus, now consider $N_{samp} = 2^{18}$ randomly generated triplets $\{J_1, J_2, J_3\}$, while keeping all the other hyperparameters unchanged. As before, we numerically evaluate the CRB from Eq. (4) starting from the Fisher information matrix of Eq. (3).

The comparison between the CRB and the estimated values is shown in Fig. 4. The error on each J_i will now depend on all three couplings $\{J_1, J_2, J_3\}$. In order to keep the consistency with the previous example, we report the error as a map of the first two couplings, for different values of the third one, one for each column of Fig. 4. As before, the surfaces indicate the CRB value, and the dots (fuchsia) are the variance $\Delta^2 J_i$ on the estimated points multiplied by the number of resources M. Panels (p)–(r) show slices of the graphs for the error on each parameter J_i, while the other two are kept at their maximum value, $J_{j,k} = 1$. The plots still show a good agreement between the estimated values and the CRB, demonstrating a nearly optimal estimation in this instance as well. This comes, however, at the cost of substantially increasing the dimension of training set, which is expected as the parameter space increases.

III. DISCUSSION

Characterizing quantum processes with the utmost attainable precision is of paramount importance in order to harness them for various tasks. Indeed, errors in the calibration would reverberate in the task at hand, hindering the reliability of the final result, and as such, they need to be validated and kept at a minimum.

Here, we have presented a multiparameter estimation-based approach for characterizing parametrized Hamiltonians, focusing on the dynamics of CTQWs. Starting solely from experimentally measurable quantities, i.e., the position distribution across the graph's sites, our method allows to perform nearly optimal estimation of the Hamiltonian parameters. We have demonstrated our approach by performing the estimation for a CTQW on a line graph for n-neighbor couplings with $n = 2$ and $n = 3$.

The estimation is carried out using a deep neural network model, which we train with data simulating experimental measured counts. These are then bootstrapped to account for Poissonian noise. Our method achieves a reliable estimation nearly saturating the CRB both for $n = 2$ and $n = 3$. We have explored the informational content of the chosen measurement strategy as a function of the graph dimension and of the evolution time at which the measurement is performed. This highlights how the measurement strategy over all sites of the graph performs better when all sites have already undergone an evolution at a fixed time. If this is not the case, localized measurements should be investigated. This also shows how, while longer times provide a higher information content, the highly structured profile of the probabilities (and hence of the FI) would impose a tighter sampling of the training set for the NN to successfully reconstruct the profile. From panels (g)–(l) of Fig. 3, we note how, while the estimated points follow closely the less-featured values of the CRB, the estimation does slightly deteriorates when there are two close features. As shown before,[22] this is also critically related to the sampling rate of the training set, which can be adjusted to attain the desired accuracy.

Our approach provides two main advantages: on the one hand, casting the problem in quantum metrological terms enables the control of the uncertainties involved in the process and their bounds, allowing to explore the informational content of Hamiltonian characterization. On the other hand, using a NN allows to perform a

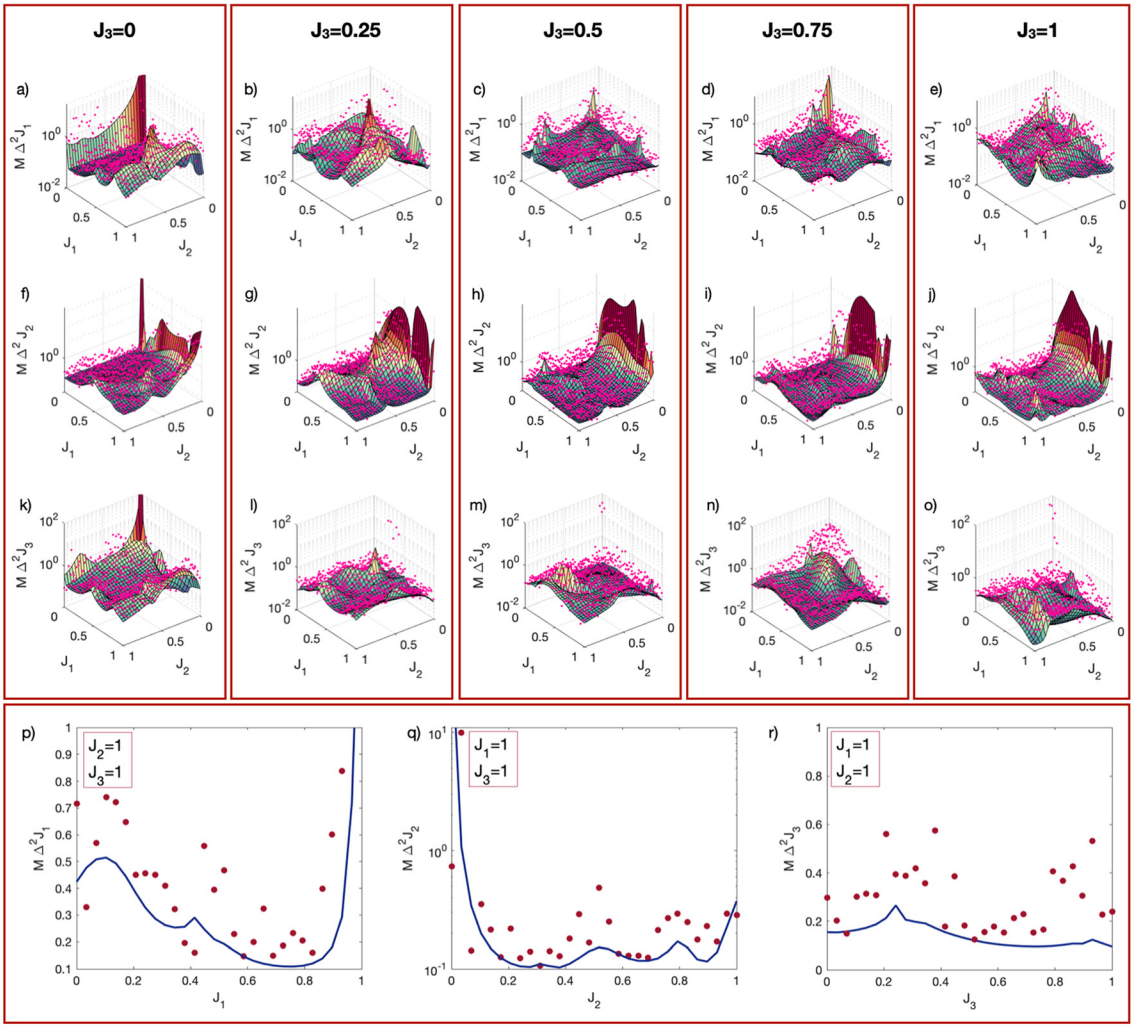

Fig. 4. Three-parameter estimation. Results of the estimation of the first, second, and third-neighbor couplings using the NN model for a fixed input state. Each 3D log-plot is a map showing the CRB (surface) and estimated variance (fuchsia circles) for $M\Delta^2 J_1$ [panels (a)–(e)], $M\Delta^2 J_2$ [panels (f)–(j)], and $M\Delta^2 J_3$ [panels (k)–(o)] as a function of J_1 and J_2 for different values of $J_3 = 0, 0.25, 0.5, 0.75,$ and 1 for each column. Panels (p)–(r) show the CRB (blue line) and evaluated variances (red circles) for $M\Delta^2 J_1$ as a function of J_1 for $J_2 = J_3 = 1$ [panel (p)], $M\Delta^2 J_2$ as a function of J_2 for $J_1 = J_3 = 1$ [panel (q)], and $M\Delta^2 J_3$ as a function of J_3 for $J_1 = J_2 = 1$ [panel (r)].

model-free estimation, which is particularly beneficial for CTQW since the probabilities are often not attainable analytically. However, both from a conceptual and a resource-based point of view, this approach is viable when the amount of parameters characterizing the CTQW is limited: the parametric estimation protocol is not an efficient way for considering a large number of parameters at once. Supervised learning is also resource-demanding in this sense, as increasing the number of parameters while keeping the estimation at the CRB requires increasing significantly the size of the training set, as it is necessary to sample each dimension in the parameter space sufficiently. While it is difficult to provide quantitative scaling of the computational resources that would be needed in a general CTQW, it can be already seen from our example that going from a two to a three-parameter estimation implied increasing the training set of roughly one order of magnitude. Depending on the computational resources at hand, this can be a strong limiting factor, although it can be mitigated by adopting well-established techniques such as batch generators. This may allow also to extend these results to multiple particles and explore more complex topologies. Degenerations in the parameter space may present when exploring more complex CTQW evolutions, but these can be resolved by measuring the probabilities at two different times, similarly to Ref. 25. While our approach does offer a certain flexibility, for large and densely connected networks, a paradigm shift may be required, and different characterization strategies may be investigated, for instance, based on search algorithms or reinforcement learning.

ACKNOWLEDGMENTS

We acknowledge M. Barbieri, M. Genoni, F. Albarelli, and M. Paris for fruitful discussion. I.G. acknowledges the support of the

project FET-OPEN-RIA STORMYTUNE (Grant Agreement No. 899587). C.B. acknowledges support from the Sviluppo UniMi 2021 initiative.

AUTHOR DECLARATIONS

Conflict of Interest

The authors have no conflicts to disclose.

Author Contributions

Ilaria Gianani: Conceptualization (equal); Data curation (lead); Formal analysis (lead); Writing – original draft (equal); Writing – review & editing (equal). **Claudia Benedetti:** Conceptualization (equal); Writing – original draft (equal); Writing – review & editing (equal).

DATA AVAILABILITY

The data that support the findings of this study are available from the corresponding author upon reasonable request.

REFERENCES

[1]J. Eisert, D. Hangleiter, N. Walk, I. Roth, D. Markham, R. Parekh, U. Chabaud, and E. Kashefi, Nat. Rev. Phys. **2**, 382 (2020).
[2]C. P. Koch, U. Boscain, T. Calarco, G. Dirr, S. Filipp, S. J. Glaser, R. Kosloff, S. Montangero, T. Schulte-Herbrüggen *et al.*, EPJ Quantum Technol. **9**, 19 (2022).
[3]A. Acín, I. Bloch, H. Buhrman, T. Calarco, C. Eichler, J. Eisert, D. Esteve, N. Gisin, S. J. Glaser *et al.*, New J. Phys. **20**, 080201 (2018).
[4]V. Dunjko and H. J. Briegel, Rep. Prog. Phys. **81**, 074001 (2018).
[5]G. Torlai and R. G. Melko, Annu. Rev. Condens. Matter Phys. **11**, 325 (2020).
[6]F. Vernuccio, A. Bresci, V. Cimini, A. Giuseppi, G. Cerullo, D. Polli, and C. M. Valensise, Laser Photonics Rev. **16**, 2100399 (2022).
[7]G. Carleo and M. Troyer, Science **355**, 602 (2017).
[8]A. Bohrdt, S. Kim, A. Lukin, M. Rispoli, R. Schittko, M. Knap, M. Greiner, and J. Léonard, Phys. Rev. Lett. **127**, 150504 (2021).
[9]B. Flynn, A. A. Gentile, N. Wiebe, R. Santagati, and A. Laing, New J. Phys. **24**, 053034 (2022).
[10]I. L. Gutiérrez and C. B. Mendl, Quantum **6**, 627 (2022).
[11]M. Papič and I. de Vega, Phys. Rev. A **105**, 022605 (2022).
[12]D. Koutný, L. Motka, Z. Hradil, J. Řeháček, and L. L. Sánchez-Soto, Phys. Rev. A **106**, 012409 (2022).
[13]E. Flurin, L. S. Martin, S. Hacohen-Gourgy, and I. Siddiqi, Phys. Rev. X **10**, 011006 (2020).
[14]G. Koolstra, N. Stevenson, S. Barzili, L. Burns, K. Siva, S. Greenfield, W. Livingston, A. Hashim, R. K. Naik *et al.*, Phys. Rev. X **12**, 031017 (2022).
[15]S. Mavadia, V. Frey, J. Sastrawan, S. Dona, and M. J. Biercuk, Nat. Commun. **8**, 14106 (2017).
[16]M. Y. Niu, S. Boixo, V. N. Smelyanskiy, and H. Neven, npj Quantum Inf. **5**, 33 (2019).
[17]A. Fallani, M. A. C. Rossi, D. Tamascelli, and M. G. Genoni, PRX Quantum **3**, 020310 (2022).
[18]T. Huang, Y. Ban, E. Y. Sherman, and X. Chen, Phys. Rev. Appl. **17**, 024040 (2022).
[19]R. Porotti, D. Tamascelli, M. Restelli, and E. Prati, Commun. Phys. **2**, 61 (2019).
[20]J. Brown, P. Sgroi, L. Giannelli, G. S. Paraoanu, E. Paladino, G. Falci, M. Paternostro, and A. Ferraro, New J. Phys. **23**, 093035 (2021).
[21]A. Lumino, E. Polino, A. S. Rab, G. Milani, N. Spagnolo, N. Wiebe, and F. Sciarrino, Phys. Rev. Appl. **10**, 044033 (2018).
[22]V. Cimini, I. Gianani, N. Spagnolo, F. Leccese, F. Sciarrino, and M. Barbieri, Phys. Rev. Lett. **123**, 230502 (2019).
[23]Y. Ming, C.-T. Lin, S. D. Bartlett, and W.-W. Zhang, npj Comput. Mater. **5**, 88 (2019).
[24]M. Valeri, E. Polino, D. Poderini, I. Gianani, G. Corrielli, A. Crespi, R. Osellame, N. Spagnolo, and F. Sciarrino, npj Quantum Inf. **6**, 92 (2020).
[25]V. Cimini, E. Polino, M. Valeri, I. Gianani, N. Spagnolo, G. Corrielli, A. Crespi, R. Osellame, M. Barbieri *et al.*, Phys. Rev. Appl. **15**, 044003 (2021).
[26]Y. Ban, J. Echanobe, Y. Ding, R. Puebla, and J. Casanova, Quantum Sci. Technol. **6**, 045012 (2021).
[27]A. M. Palmieri, F. Bianchi, M. G. A. Paris, and C. Benedetti, Phys. Rev. A **104**, 052412 (2021).
[28]I. Gianani, I. Mastroserio, L. Buffoni, N. Bruno, L. Donati, V. Cimini, M. Barbieri, F. S. Cataliotti, and F. Caruso, Adv. Quantum Technol. **5**, 2100140 (2022).
[29]C. E. Granade, C. Ferrie, N. Wiebe, and D. G. Cory, New J. Phys. **14**, 103013 (2012).
[30]N. Wiebe, C. Granade, C. Ferrie, and D. G. Cory, Phys. Rev. Lett. **112**, 190501 (2014).
[31]N. Wiebe, C. Granade, C. Ferrie, and D. Cory, Phys. Rev. A **89**, 042314 (2014).
[32]C. Cao, S.-Y. Hou, N. Cao, and B. Zeng, J. Phys.: Condens. Matter **33**, 064002 (2020).
[33]L. Che, C. Wei, Y. Huang, D. Zhao, S. Xue, X. Nie, J. Li, D. Lu, and T. Xin, Phys. Rev. Res. **3**, 023246 (2021).
[34]D. Rattacaso, G. Passarelli, and P. Lucignano, Quantum **7**, 905 (2023).
[35]J. Wang, S. Paesani, R. Santagati, S. Knauer, A. A. Gentile, N. Wiebe, M. Petruzzella, J. L. O'Brien, J. G. Rarity *et al.*, Nat. Phys. **13**, 551 (2017).
[36]A. A. Gentile, B. Flynn, S. Knauer, N. Wiebe, S. Paesani, C. E. Granade, J. G. Rarity, R. Santagati, and A. Laing, Nat. Phys. **17**, 837 (2021).
[37]V. Giovannetti, S. Lloyd, and L. Maccone, Science **306**, 1330 (2004).
[38]V. Giovannetti, S. Lloyd, and L. Maccone, Nat. Photonics **5**, 222 (2011).
[39]M. G. A. Paris, Int. J. Quantum Inf. **7**, 125 (2009).
[40]M. Barbieri, PRX Quantum **3**, 010202 (2022).
[41]F. Albarelli, M. Barbieri, M. Genoni, and I. Gianani, Phys. Lett. A **384**, 126311 (2020).
[42]M. B. Plenio and S. F. Huelga, New J. Phys. **10**, 113019 (2008).
[43]O. Mülken and A. Blumen, Phys. Rep. **502**, 37 (2011).
[44]C. Uchiyama, W. J. Munro, and K. Nemoto, npj Quantum Inf. **4**, 33 (2018).
[45]A. M. Childs and J. Goldstone, Phys. Rev. A **70**, 022314 (2004).
[46]J. K. Gamble, M. Friesen, D. Zhou, R. Joynt, and S. N. Coppersmith, Phys. Rev. A **81**, 052313 (2010).
[47]S. Chakraborty, L. Novo, and J. Roland, Phys. Rev. A **102**, 032214 (2020).
[48]Y. Atia and S. Chakraborty, Phys. Rev. A **104**, 032215 (2021).
[49]M. G. A. Paris, C. Benedetti, and S. Olivares, Symmetry **13**, 96 (2021).
[50]A. Candeloro, C. Benedetti, M. G. Genoni, and M. G. A. Paris, Adv. Quantum Technol. **6**, 2200093 (2023).
[51]S. Apers, S. Chakraborty, L. Novo, and J. Roland, Phys. Rev. Lett. **129**, 160502 (2022).
[52]A. M. Childs, Phys. Rev. Lett. **102**, 180501 (2009).
[53]N. B. Lovett, S. Cooper, M. Everitt, M. Trevers, and V. Kendon, Phys. Rev. A **81**, 042330 (2010).
[54]A. M. Childs, D. Gosset, and Z. Webb, Science **339**, 791 (2013).
[55]S. Bose, Contemp. Phys. **48**, 13 (2007).
[56]E. Farhi and S. Gutmann, Phys. Rev. A **58**, 915 (1998).
[57]J. Kempe, Contemp. Phys. **44**, 307 (2003).
[58]S. E. Venegas-Andraca, Quantum Inf. Process. **11**, 1015 (2012).
[59]K. Kadian, S. Garhwal, and A. Kumar, Comput. Sci. Rev. **41**, 100419 (2021).
[60]O. Mülken, V. Bierbaum, and A. Blumen, J. Chem. Phys. **124**, 124905 (2006).
[61]A. Kay, Int. J. Quantum Inf. **8**, 641 (2010).
[62]C. Chudzicki and F. W. Strauch, Phys. Rev. Lett. **105**, 260501 (2010).
[63]V. M. Kendon and C. Tamon, J. Comput. Theor. Nanosci. **8**, 422 (2011).
[64]R. Alvir, S. Dever, B. Lovitz, J. Myer, C. Tamon, Y. Xu, and H. Zhan, J. Algebraic Combinatorics **43**, 801 (2016).
[65]S. Cavazzoni, L. Razzoli, P. Bordone, and M. G. A. Paris, Phys. Rev. E **106**, 024118 (2022).
[66]G. Maquiné Batalha, A. Volta, W. T. Strunz, and M. Galiceanu, Sci. Rep. **12**, 6896 (2022).
[67]X. Qiang, T. Loke, A. Montanaro, K. Aungskunsiri, X. Zhou, J. L. O'Brien, J. B. Wang, and J. C. F. Matthews, Nat. Commun. **7**, 11511 (2016).

[68]H. Tang, X.-F. Lin, Z. Feng, J.-Y. Chen, J. Gao, K. Sun, C.-Y. Wang, P.-C. Lai, X.-Y. Xu *et al.*, Sci. Adv. **4**, eaat3174 (2018).
[69]P. Imany, N. B. Lingaraju, M. S. Alshaykh, D. E. Leaird, and A. M. Weiner, Sci. Adv. **6**, eaba8066 (2020).
[70]E. J. Meier, F. A. An, and B. Gadway, Phys. Rev. A **93**, 051602 (2016).
[71]M. Tamura, T. Mukaiyama, and K. Toyoda, Phys. Rev. Lett. **124**, 200501 (2020).
[72]H. B. Perets, Y. Lahini, F. Pozzi, M. Sorel, R. Morandotti, and Y. Silberberg, Phys. Rev. Lett. **100**, 170506 (2008).
[73]K. Poulios, R. Keil, D. Fry, J. D. A. Meinecke, J. C. F. Matthews, A. Politi, M. Lobino, M. Gräfe, M. Heinrich *et al.*, Phys. Rev. Lett. **112**, 143604 (2014).
[74]F. Caruso, A. Crespi, A. G. Ciriolo, F. Sciarrino, and R. Osellame, Nat. Commun. **7**, 11682 (2016).
[75]C. Benedetti, D. Tamascelli, M. G. Paris, and A. Crespi, Phys. Rev. Appl. **16**, 054036 (2021).
[76]J. Böhm, M. Bellec, F. Mortessagne, U. Kuhl, S. Barkhofen, S. Gehler, H.-J. Stöckmann, I. Foulger, S. Gnutzmann *et al.*, Phys. Rev. Lett. **114**, 110501 (2015).
[77]J. Du, H. Li, X. Xu, M. Shi, J. Wu, X. Zhou, and R. Han, Phys. Rev. A **67**, 042316 (2003).
[78]M. Christandl, N. Datta, A. Ekert, and A. J. Landahl, Phys. Rev. Lett. **92**, 187902 (2004).
[79]C. Albanese, M. Christandl, N. Datta, and A. Ekert, Phys. Rev. Lett. **93**, 230502 (2004).
[80]A. Zwick, G. A. Álvarez, J. Stolze, and O. Osenda, Phys. Rev. A **84**, 022311 (2011).
[81]A. Zwick, G. A. Álvarez, G. Bensky, and G. Kurizki, New J. Phys. **16**, 065021 (2014).
[82]Z. Zimborás, M. Faccin, Z. Kádár, J. D. Whitfield, B. P. Lanyon, and J. Biamonte, Sci. Rep. **3**, 2361 (2013).
[83]D. Lu, J. D. Biamonte, J. Li, H. Li, T. H. Johnson, V. Bergholm, M. Faccin, Z. Zimborás, R. Laflamme *et al.*, Phys. Rev. A **93**, 042302 (2016).
[84]M. Frigerio, C. Benedetti, S. Olivares, and M. G. A. Paris, Phys. Rev. A **104**, L030201 (2021).
[85]A. Khalique, A. Sett, J. Wang, and J. Twamley, New J. Phys. **23**, 083005 (2021).
[86]M. G. A. Frigerio and M. Paris, "Swift chiral quantum walks," arXiv:2207.05168 (2022).
[87]Y.-G. Yang, Q.-X. Pan, S.-J. Sun, and P. Xu, Sci. Rep. **5**, 7784 (2015).
[88]A. A. Abd EL-Latif, B. Abd-El-Atty, and S. E. Venegas-Andraca, Opt. Laser Technol. **116**, 92 (2019).
[89]A. A. Abd-EL-Latif, B. Abd-El-Atty, and S. E. Venegas-Andraca, Physica A **547**, 123869 (2020).
[90]D. Tamascelli, C. Benedetti, S. Olivares, and M. G. A. Paris, Phys. Rev. A **94**, 042129 (2016).
[91]L. Seveso, C. Benedetti, and M. G. A. Paris, J. Phys. A **52**, 105304 (2019).
[92]I. Gianani, M. G. Genoni, and M. Barbieri, IEEE J. Select. Top. Quantum Electron. **26**, 19603233 (2020).
[93]J. Spall, IEEE Control Syst. Mag. **23**, 34 (2003).
[94]P. E. Jacob, J. O'Leary, and Y. F. Atchadé, J. R. Stat. Soc., B **82**, 543 (2020).